

Real-time Motion Detection Algorithms for Spherical Navigator Echoes in Functional MRI

N. Ari¹, R. A. Kraft²

¹GE Healthcare, Waukesha, WI, United States, ²Biomedical Engineering, Wake Forest University, Winston-Salem, NC, United States

INTRODUCTION: Functional MRI detects small signal changes therefore it is very sensitive to head motion. One way to compensate for motion is using spherical navigator echo (SNAV) that samples a spherical shell in k-space to track head position [1]. The SNAV technique is ideal for prospective motion correction in fMRI: it has very short acquisition times, robust algorithms are readily available (motion detection), and imaging coordinates can be updated quickly on MR scanners (motion correction). However, current algorithms require significant computation times and this shortcoming limits the feasibility of SNAV. We developed a new method for SNAV, optimized to have a motion detection accuracy of $0.3mm$ and timing performance of $2300ms$ for a TR of $2500ms$. This optimized method is based on decoupling rotations and translations using Fourier Transform (FT) properties. Then, we developed k-space thresholded Least Squares Conjugate Gradient (kt-LSCG) algorithm for translation detection, and multi-scale DownHill Simplex (ms-DHS) algorithm with normalized Least Squares (nLS) cost function for rotation detection.

THEORY: Motion detection with SNAV can be simplified by decoupling rotation and translation, which allows application of faster algorithms for each component. Two FT properties make this possible [2]: (1) translation corresponds to linear phase shift in k-space, thus can be detected using only SNAV phase, (2) rotation corresponds to rotation by same angle in k-space, thus can be detected using only SNAV magnitude. This decoupling process works only if rotation detection is performed first, followed by translation detection. Rotation detection with SNAV is similar to registration of two images projected on a spherical surface. If spherical images are S_r (reference SNAV) and S_f (floating SNAV), then registration problem is to find the best geometric alignment with respect to the features of S_r and S_f , shown in Figure 1. SNAV registration is straightforward provided that there are sufficient features and the spherical shells are sampled densely enough. Rotation detection becomes constructing a cost function that measures the similarity between S_f and S_r , and searching for the rotation angle that minimizes this cost function. After rotations are corrected, translations can be detected by measuring the phase difference between S_r and S_f at the corrected position. The phase change between S_r and S_f is measured using EQ1: $\Delta\phi = \arg\{S_f\} - \arg\{S_r\} = 2\pi/\kappa(kx.\Delta x + ky.\Delta y + kz.\Delta z)$. The EQ1 states that displacement vector $(\Delta x, \Delta y, \Delta z)$ in spatial domain is proportional to slope of the phase change $(\Delta\phi)$ in k-space. Theoretically, only 3 points of SNAV is sufficient (there are 3 unknowns) to solve EQ1. However, all SNAV samples should be used to obtain a robust estimation against noisy data. If SNAV has N points, translation detection becomes solving linear system of N equations with 3 unknowns.

METHODS: Rotations were detected using ms-DHS algorithm with nLS cost function. The DHS [3] requires only function evaluations, not derivatives; hence it converges quickly for this multi-dimensional problem. The DHS applies trial rotations to S_f while searching for the minimum of nLS. The crucial step of DHS is optimization of 3D interpolation for determining S_t (trial SNAV), after a "trial" rotation is applied to S_f . Our interpolation works as: 1) Transform 3D Cartesian coordinates (x, y, z) of SNAV to 2D latitude and longitude coordinates (ϕ, θ) . 2) Perform 2D Delaunay triangulation to generate triangular meshes of non-uniformly sampled SNAV in (ϕ, θ) coordinates. 3) Find enclosing Delaunay triangle, using the triangular meshes, for each S_t sample. 4) Compute magnitude values of S_t by interpolating three S_f samples that are corresponding vertices of the enclosing triangle. Once S_t samples calculated, the nLS cost function was computed to quantify the similarity between S_r and S_t . Our nLS implementation first applied a global scaling by normalization of S_r and S_t with a constant scaling factor. Second, a voxel-by-voxel weighting was applied. Mathematically: $nLS(X, Y) = \sum [c1.w1_i.X_i - c2.w2_i.Y_i]^2$, where $c1, c2$ are constant scaling factors and $w1, w2$ are weighting vectors to selectively assign significance to various parts of SNAV data. We used $mean\{S_r\}$ and $mean\{S_f\}$ for global scaling, and magnitude vector of S_r as weighting vectors. Finally, the DHS algorithm was used to find the minimum of nLS function. However, DHS does not guarantee finding a global minimum. Therefore, DHS should be restarted with a new random starting simplex to make sure we are finding the global minimum. The recursive iteration scheme can significantly slow down the DHS. We developed a multi-scale DHS, which performs function evaluations for minimization at a high scale by sub-sampling S_f to improve speed, but performs interpolations at a lower scale without sub-sampling S_r to improve accuracy. To further improve the speed, we used a restricted parameter space to perform ms-DHS. This process is shown in Figure 2. Translations were detected using kt-LSCG algorithm that applies k-space SNR threshold before solving EQ1 to provide a smooth variation between phases of adjacent SNAV samples. Our implementation used formula in EQ2: $T = mean\{S_r\} / \lambda$, where λ is a user defined threshold parameter. After thresholding, over-determined system of equations EQ3: $Ax = b$ was formed using EQ1, where vector b contains phase differences of S_r and S_f , matrix A contains k-space position of each SNAV sample (kx, ky, kz) , and vector x contains unknowns $(\Delta x, \Delta y, \Delta z)$. We solved EQ3 using a time efficient LSCG algorithm [3] that solves least squares problem $min\|b - Ax\|_2$ by applying conjugate gradients to the normal equations $A^*Ax = A^*b$. The LSCG is an iterative method and converges quickly for this over-determined problem. Before applying kt-LSCG, a phase unwrapping algorithm was applied to replace absolute phase jumps greater than π to their 2π complements. These radian phase jumps were introduced by subtraction of the raw phases of S_r and S_f , and a modulus operator was applied to wrap these large phase differences. Figure 3 illustrates steps performed to prepare SNAV data: a) raw phase difference plot illustrates radian phase jumps greater than π , b) phase unwrapping algorithm folds phase differences between S_r and S_t into range $\pm\pi$, c) thresholding removes all the noisy data to improve accuracy of LSCG algorithm.

RESULTS and DISCUSSIONS: To demonstrate feasibility of our technique, we integrated SNAV sequence into EPI sequence, and performed MR experiments with phantom located on a motion platform. The motion platform systematically rotates the phantom within $\pm 10^\circ$ range along the vertical axis for rotation detection, and translates the phantom within $\pm 10mm$ range along the bore of MR scanner for translation detection experiments. One SNAV was acquired at each position of the phantom and ms-DHS with nLS cost function was used to estimate rotations, and kt-LSCG algorithm was used to estimate translations. SNAV detected motion with high accuracy: group average for absolute error was 0.19° for rotations, and $0.23mm$ for translations, all within the precision of motion platform. Detected rotations (translations) versus applied rotations (translations) were plotted in Figure 4. We demonstrated that SNAV can be used to perform real-time motion detection with high accuracy in less than $2500ms$.

REFERENCES: [1] EB Welch, *Mag Res Med*, 47:32, 2002. [2] RN Bracewell, *The Fourier Transform And Its Applications*, 1999. [3] J Nocedal, *Numerical Optimization*, 1999.

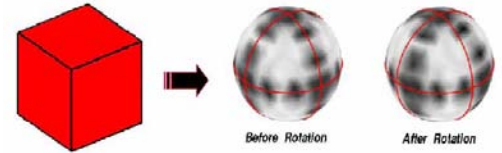


Figure 1: Magnitude plots of simulated SNAVs in the kspace of a 3-D uniform cubic object before and after a 20° rotation of the cube in the image domain.

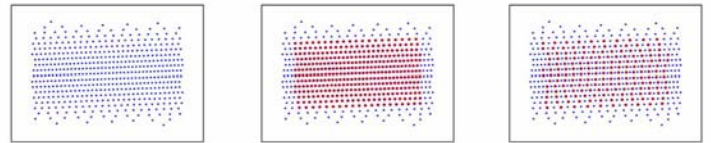


Figure 2: Multi-scale simplex minimization. We obtain triangular meshes using all the scattered samples of S_r . For floating SNAV (left), first the parameter space is restricted (middle), then S_f is sub-sampled to improve speed (right).

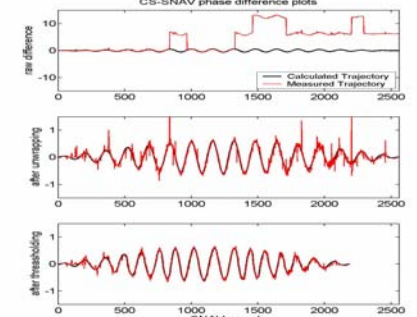


Figure 3: Phase difference plots of SNAVs from in vitro data: a) raw phase difference, b) after unwrapping, c) after thresholding.

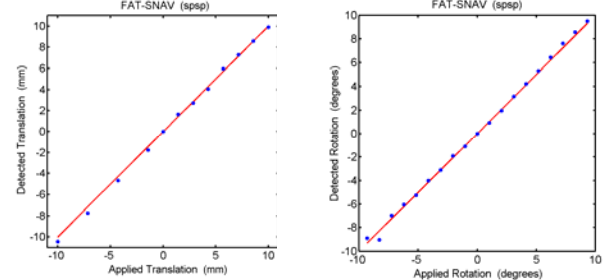


Figure 4: Translation and rotation detection accuracy of SNAV technique for MR phantom study.